Nanoscale

PAPER

Electronic Structure Characterization of Individual Single-walled Carbon Nanotube by *in situ* Electrochemical Surface-enhanced Raman Scattering Method

Received 00th January 20xx,
Accepted 00th January 20xx

DOI: 10.1039/x0xx00000x

www.rsc.org/

Satoshi Yasuda,[a] Shinji Hoshina,[a] Shohei Chiashi,[b] Shigeo Maruyama,[b] and Kei Murakoshi*[a]

We present an electronic structural analysis of an individual single-walled carbon nanotube (SWNT) employing electrochemical surface-enhanced Raman scattering (SERS). An isolated SWNT was supported on a well-defined Au nanodimer structure, which possesses a localized surface plasmon resonance (LSPR) field at the nanogap, and highly intense SERS spectra were measured for the SWNT at the gap region. The absolute potential of the Fermi level of the isolated SWNT in an ionic liquid was determined from the electrochemical potential dependence of the SERS intensity showing the dependence on the chirality of SWNT. The electronic structural change in an isolated SWNT by ozone oxidation treatment was also analyzed. The results indicate that the electrochemical SERS technique is a powerful tool for detailed analysis of the electronic structure of isolated SWNTs.

Introduction

Single-walled carbon nanotubes (SWNTs) have a one dimensional cylindrical graphitic structure and are fascinating nanomaterials due to their quasi-one-dimensionality.[1,2] The specific structure gives rise to several spiked density of states, which correspond to the van Hove singularities (VHSs), and consequently produces a band gap between subbands arising from the VHSs. In addition, SWNTs exhibit either metallic or semiconducting character, which is dependent on the chirality of the SWNT. Several recent studies indicated that geometric defects and heteroatom doping of a SWNT significantly enhances the photo, electronic, catalytic and chemical properties of SWNTs, which has further expanded the potential of SWNTs as advanced nanomaterials.[3–7]

The absolute potential of the structure-dependent energy level is one of the fundamental parameters to determine electron transfer ability, and thus a detailed understanding of the local electronic structure is required to improve and design SWNT-based advanced materials. Among the various types of nano-analysis techniques, scanning probe microscopies have been widely employed to probe local electronic structures. Kelvin force microscopy provided information on the local surface potential of individual SWNTs, which is related to the local work function.[8,9] Electrochemical scanning tunneling spectroscopy has been used to determine the local absolute potential of the Fermi energy for individual SWNTs at the nanometer scale.[10] Although single SWNT measurements have been successfully demonstrated, the scanning probe techniques inherently suffer from not only low throughput, but also difficulties in fixing the probe position for the target.

Resonance Raman scattering (RRS) and photoluminescence (PL) techniques are other useful methodologies for investigation of the electronic structures of individual SWNTs. Strong RRS and PL due to the optical transition between VHSs enables the detection of spectra with high throughput and sensitivity. Several groups have thus determined the absolute potential of the valence and conduction bands, and the Fermi levels for individual semiconducting SWNTs by the PL method, whereby the Fermi level was found to be dependent on the SWNT diameter.[11,12] Although significant information related to the electronic state could be successfully obtained, it was not local at the nanometer level but averaged results from bulk SWNTs dispersed in solution. In addition to the PL method, the electrochemical Raman scattering method was also employed to probe the electronic state of individual SWNTs in detail.[13] Raman spectra of single SWNTs can be analyzed due to the RRS process. Furthermore, unlike the PL method, RRS enables Raman spectra of both metallic and semiconducting SWNTs to be measured, which allows the analysis of both electronic states of individual SWNTs. Analysis of the electrochemical potential dependence of the Raman intensity enabled the absolute potential of the Fermi level to be determined for both metallic and semiconducting individual SWNTs.[14] Generally, due to the diffraction limit of light in sub-micrometer region, the contribution of the local electronic structure has not yet been clarified using confocal Raman scattering measurement.

[a] Department of Chemistry, Faculty of Science, Hokkaido University, Sapporo, Hokkaido 060-0810, Japan.
[b] Department of Mechanical Engineering, The University of Tokyo, Bunkyo-ku, Tokyo 113-8656, Japan
E-mail: kei@sci.hokudai.ac.jp

Surface-enhanced Raman scattering (SERS) is a phenomenon that significantly enhances Raman scattering due to the localized surface plasmon resonance (LSPR) field in the vicinity of metal nanostructures under light illumination. In particular, a metal nanodimer structure with a nanogap produces a strong LSPR field at the gap due to coupling of the LSPR excitation of the metal structures. The intense LSPR field condensed within the nanometer region enables strong and highly localized Raman scattering detection of target at the nanometer level with very high throughput and sensitivity.[15–21] Recently, an isolated SWNT was supported within a Au dimer gap, and intense SERS spectra for the nano-gap region of the isolated SWNT could be successfully detected.[22] In addition, strong coupling of LSPR with a SWNT was found to cause selection-rule breakdown in the electronic optical transitions of the SWNT.[23] In spite of the progresses in the use of LSPR for the characterization, determination of the local electronic structure *in-situ* has not yet been carried out.

Herein, we present validation of the electrochemical SERS technique for analysis of the electronic state of individual SWNTs. An individual SWNT was supported on a well-defined Au nanodimer structure with an intense LSPR field, and SERS spectra were measured for the nanometer region of the isolated SWNT. The electrochemical dependence of the SERS spectra demonstrated that the absolute potential of the Fermi level for an isolated SWNT could be analyzed, and a relationship between the tube diameter and the Fermi level was established. The change in the dependence of the potential on the SERS intensity, induced by ozone oxidation treatment, was also evaluated.

Experimental

Well-defined Au nanodimer arrays were fabricated using the angle-resolved nanosphere lithography technique (AR-NSL)[16,24] to obtain an optimum LSPR field. Au nanodimer arrays with a maximum extinction peak around 800 nm for incident light parallel to the long axis of the dimer were fabricated over indium tin oxide (ITO) coated on glass because a He-Ne laser with a wavelength of 785 nm was used for the excitation of Raman scattering. SWNT, which was synthesized by alcohol chemical vapor deposition and provided by Prof. Maruyama, was used.[25] 100 μg of SWNTs was ultrasonicated in 10 mL of 1,2-dichloromethane for 1.5 h, followed by centrifugation for 30 min to remove excess SWNT bundles. The supernatant was diluted in 10 mL of 1,2-dichloromethane, and the ultrasonicated solution was dispersed onto the Au nanodimer array on the ITO substrate. After deposition, rinsing with Milli-Q water was repeatedly performed to remove excess SWNTs. This simple dispersion process can support an isolated SWNT at the Au nanodimer array, as reported previously.[22,23] The incident polarization dependence of the SERS signal intensity confirms that the SWNTs exhibit SERS in the Au nanogap.[22,23] Confocal micro Raman spectroscopy was employed under electrochemical control (Renishaw 2000 spectrometer) with a 785 nm wavelength excitation laser using a 100× objective lens. *N*,*N*,*N*-trimethyl-N-propylammonium bis-(trifluromethane sulfonyl) imide (TMPA-TFSI, Kanto Chemical), which is a representative ionic liquid, was used as an electrolyte because it has a wide electrochemical window and is easily dehydrated. Heat treatment was conducted at 120 °C for 24 h in a vacuum oven (ca. 10^4 Pa) to remove water. An Ag/Ag^+ electrode in saturated $AgSO_3CF_3$ (99.5% Wako) in TMPA-TFSI was used as a reference electrode. Pt wire was used as a counter electrode.

Results and discussion

Figure 1(a) shows a representative RRS spectrum obtained for bundled SWNTs deposited on glass. Three dominant Raman features were observed, which are attributed to the radial breathing mode (RBM) at low frequency region, and the *D* band (ca. 1300 cm^{-1}) and *G* band (ca. 1590 cm^{-1}) modes. The RBM frequency arises from coherent bond-stretching in the radial direction and is inversely proportional to the tube diameter. The *D* band is related to defect structures in the graphene matrix and is an indicator of disorder. The *G* band is attributed to the in-plane C-C bond stretching mode of the graphene lattice structure, and splits into G^+ and G^- modes at higher and lower Raman frequencies, which originate from along the tube axis and along the tube circumference axis, respectively. From the observed RBM frequencies, the diameter, chirality and electronic character (semiconducting or metallic) of a SWNT can be identified. Analysis of the relationship between several observed RBM frequencies and the excitation laser energy, i.e., a Kataura plot,[26,27] indicated the coexistence of both semiconducting and metallic SWNTs with diameters in the range of 0.8–2.0 nm. SERS measurement was conducted for an isolated SWNT supported on a Au nanodimer array. Unlike the RRS spectrum, an intense Raman signal could be clearly observed (Figure 1(b)). Typical RBM intensities were four or more times stronger than the RRS spectrum for the isolated SWNT. A single narrow RBM peak at 230 cm^{-1} clearly indicates that the measured SWNT is an individual SWNT. According to the Kataura plot,[26,27] the observed SWNT could be easily assigned to an isolated (8,7)

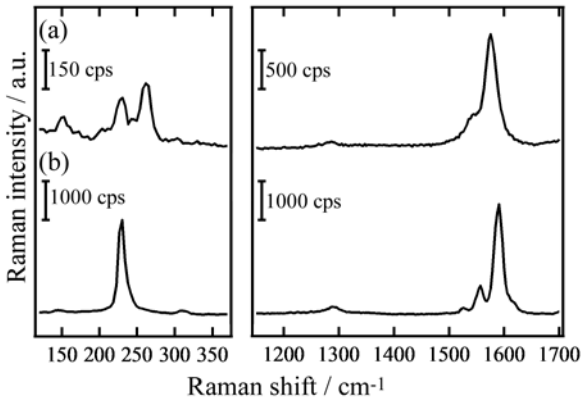

Fig. 1 (a) RRS spectrum obtained for bundled SWNTs deposited on glass. (b) SERS spectrum for an isolated (8,7) SWNT with an RBM of 230 cm^{-1} supported on a Au nanodimer structure.

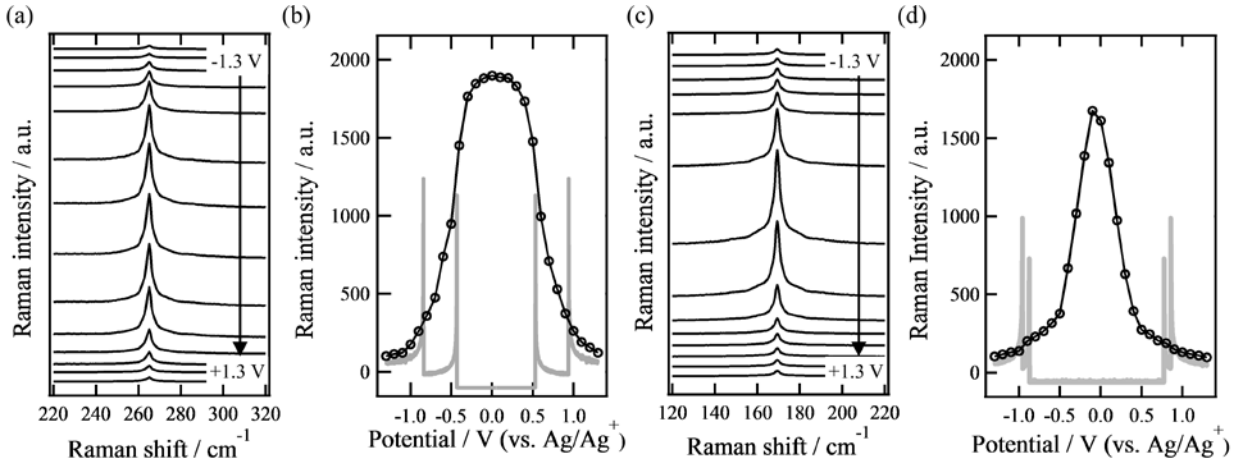

Fig. 2 RBM SERS spectra under different potentials and plot of the RBM SERS intensity against the potential for (a, b) an isolated semiconducting SWNT with an RBM of 265 cm^{-1}, and (c, d) an isolated metallic SWNT with an RBM of 169 cm^{-1}.

semiconducting SWNT with a diameter of 1.03 nm. Using such a substrate, the electrochemical potential dependence of the SERS spectra was evaluated for isolated semiconducting and metallic SWNTs at the nanometer scale.

Figure 2(a) shows RBM Raman spectra at 265 cm^{-1} for an isolated (10,2) semiconducting SWNT acquired with different electrochemical potentials. The peak intensities were clearly dependent on the potential and had a maximum at a certain potential with an intensity plateau, as shown by the RBM intensity versus potential plot (Fig. 2(b)). The same analysis was also conducted for an isolated metallic SWNT (Fig. 2(c)), although the RBM frequency was assigned to a (18,0) or (17,2) metallic SWNT. The RBM intensities followed a similar trend with respect to the potential, but no intensity plateau was observed (Fig. 2(d)).

Previous reports on the potential dependence of the RBM intensity proposed that the observed trend can be attributed to doping to the conduction band and undoping to the valence band of the SWNT.[13,14,28,29] The doping and undoping processes cause a shift of the Fermi level to higher and lower potentials, respectively. Bleaching of the optical transition between VHSs occurs as the number of electrons in the density of state (DOS) changes; therefore, the resonant Raman intensity decreases. The resultant RBM intensity profile showed a maximum peak at the potential where the Fermi level is attained at the mid-gap energy between the first VHSs of the SWNT due to maximum resonance. Considering that the electrochemical potential with maximized Raman intensity corresponds to the absolute potential of the Fermi level of the SWNT, which is located in the mid-gap between the first VHSs, the DOSs calculated for both SWNTs reported previously were superimposed as gray lines in Figs. 2(b) and (d).[30] It is clear that the potential dependence of the RBM intensity for the semiconducting SWNT (Fig. 2(b)) had a plateau and dropped to around half of the calculated VHSs in the DOS, while sharp attenuation of the RBM intensity was observed for the metallic SWNT (Fig. 2(d)). Such different trends for these SWNTs are in good agreement with the previous results,[13] which indicates that the electronic character can be identified from in situ electrochemical SERS spectra as well as RSS spectra. The potential maximized Raman intensity *E*, was evaluated to be 0.0 and -0.1 V vs. Ag/Ag^+ for the semiconducting and metallic SWNTs, respectively, and the absolute potentials of the Fermi level ϕ_{abs}, were estimated based on the following equation:[31]

$$\phi_{abs} \text{ (vs. vacuum)} = \phi \text{ (vs. SHE)} + 4.44 \text{ V} \qquad (1)$$

Here, we assume that observed electrode potential ϕ (vs. Ag/Ag^+) corresponds to that of 0.01 M Ag/Ag^+ reference electrode in acetonitrile with the value of 0.560 V to ϕ (vs. standard hydrogen electrode (SHE)).[32] The ϕ (vs. Ag/AgCl (Sat. KCl)) = ϕ (vs. SHE) – 0.199 V is also used in Fig. 3 to compare previously reported values. ϕ_{abs} is dependent on the diameter of the SWNT. Figure 3 shows the RBM Raman shift (diameter) dependence of ϕ_{abs} for individual SWNTs. The estimated local ϕ_{abs} are marked as red solid circles. Previously reported results are also denoted as black circles obtained by electrochemical Raman measurements for an isolated SWNT,[14] and black triangles and squares represent data obtained with electrochemical PL methods.[11,12] In the region of 140–180 cm^{-1}, the RBM frequencies for the metallic SWNT are shown, and the SWNTs are semiconducting in the range of 200 to 320 cm^{-1}. It should be noted that unlike the PL method, the Raman scattering method can be used to analyze both semiconducting and metallic SWNTs. Figure 3 shows that the present results have a tendency where ϕ_{abs} decreases as the SWNT diameter increases, which is similar to the trend observed by the electrochemical PL method.[12] However, ϕ_{abs} estimated for the semiconducting SWNT was more positive than that obtained with RRS (black circles)[12] and other PL methods (black triangles),[9] and it showed a more gentle diameter vs. ϕ_{abs} dependence. The difference in the diameter vs. ϕ_{abs} dependence obtained in the present observations could be attributed to highly localized excitation by the LSPR field at the nanogap of the Au nanodimer for in situ electrochemical SERS measurement. The previously reported R

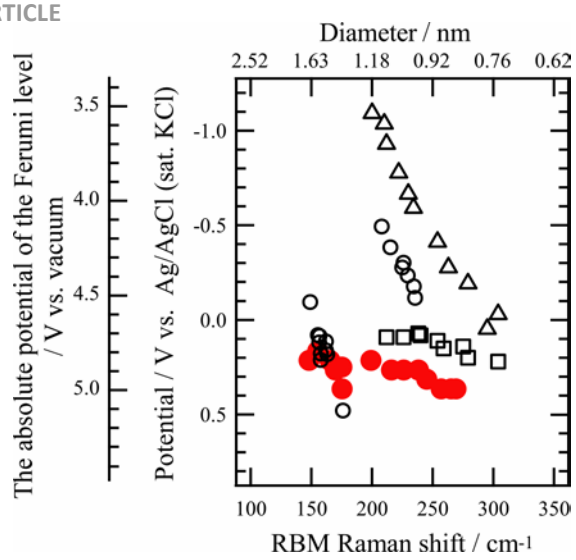

Fig. 3 RBM Raman shift (diameter) dependence of ϕ_{abs} for individual SWNTs. The estimated ϕ_{abs} are marked as red solid circles. Previously reported results are also denoted as black circles obtained by electrochemical Raman measurements for an isolated SWNT,[14] and black triangles and squares represent data obtained with electrochemical PL methods.[11,12]

RS (black circles)[14] and PL (black triangles)[11] results were based on measurements of an isolated SWNT under electron density control using electrodes and chemical species, respectively. In these experiments, the characteristics of the electronic structure reflecting averaged information of whole part of SWNTs in solution could be obtained. In the present system, it is possible to obtain information on the local electronic structures of the SWNT in the vicinity of the metal nanostructure, and thus the intrinsic properties of carbon atoms in a graphene matrix can be observed as having a relatively weak diameter dependence on the electrochemical potential of the electrons in the local density of states (LDOS).

Another previously reported PL result (black squares)[12] obtained by ensemble measurements of bundle SWNTs on an electrode shows the similarity of the present observation. The slight chirality dependences observed in both experiments may reflect the information on the LDOS of doped/undoped SWNT solvated at the electrified interface. The difference in the values of the potential at the present SERS measurement may be related to the characteristics of the solvation of SWNT in an ionic liquid. Although further analysis is necessary, we have demonstrated that the absolute potential of the Fermi level can be determined for both semiconducting and metallic isolated SWNTs by the *in situ* electrochemical SERS method.

Finally, to investigate further potential of the electrochemical SERS technique, a detailed local electronic structure analysis was also attempted for an isolated SWNT with defects. Analysis of the local electronic state of a single active site in an SWNT is strongly desired. In this study, a defect structure was produced by ozone oxidation treatment as the active site, and the modulation effect of the defect site upon the local electronic structure was evaluated by application of the electrochemical SERS technique. Ozone treatment effectively produces defect structures in SWNTs,[33–35] which activates catalytic properties.[3,36] Figure 4(a) shows SERS spectra for isolated semiconducting SWNTs before (upper) and after (lower) ozone treatment. Prior to the treatment, the *D* band, which is ascribed to the defect structure, was not clearly evident. However, an increase in the *D* band intensity was clearly observed after the ozone treatment, which indicates defect formation in the SWNT. Using the defect SWNT, the potential dependence of the RBM intensity was measured, and the results are shown in Fig. 4(b). The black open circle and solid circle symbols correspond to non-treated and ozone-treated semiconducting SWNTs, respectively. In contrast to the non-treated SWNT (black circles), the potential trend of the RBM intensity was asymmetric for the treated SWNT, and was slightly distorted around the peak at the side of positive potential region (Fig. 4(b): black solid circle symbol). This result strongly suggests a reduction of the LDOS. According to previous studies, ozone molecules react with the SWNT surface and produce epoxide moieties. X-ray photoelectron spectroscopy (XPS) analysis indicated that the π band near the Fermi level was disrupted by the oxidation process, and as a result, reduction of the electronic conductivity was induced.[33] In consideration of this result, we propose that the distorted shape corresponds to a reduction of the valence of the first VHS of the SWNT, and the

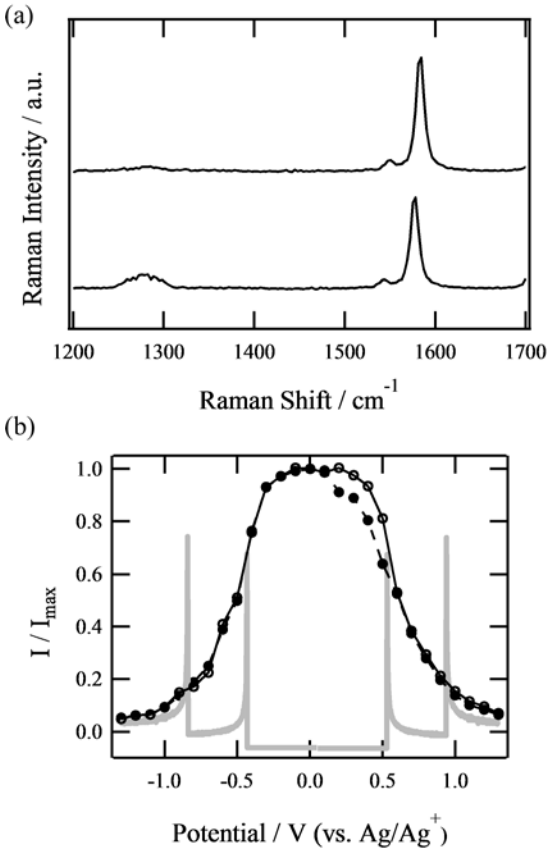

Fig. 4 (a) SERS spectra for an isolated semiconducting SWNT before (upper) and after (lower) ozone treatment. (b) Potential dependence of the RBM intensity before and after the treatment.

change in the local electronic structure in the valence π band can be probed via the electrochemical SERS method.

Conclusions

We presented a study on the electronic structure of individual SWNT using an in situ electrochemical SERS method. A relationship between the SWNT diameter and the absolute potential of the Fermi level was also determined, which indicates that the present method can provide information on the local electronic structures of a SWNT in the vicinity of a metal nanostructure. Changes in the local electronic state of the SWNT induced by ozone oxidation treatment were also probed. The change in the LDOS could be attributed to highly localized reduction of the π band in the VHS. These findings strongly indicate that the electrochemical SERS technique is a powerful tool for the investigation of local electronic structures in SWNTs, and it could serve useful for the design and developing development of advanced SWNT-based devices.

Acknowledgements

This work was supported by Grants-in-Aid for Scientific Research (Nos. 26248001 and 24655162) from the Ministry of Education, Culture, Sports, Science, and Technology of Japan.

References

1 S. Iijima, *Nature*, 1991, **354**, 56–58.

2 S. Iijima and T. Ichihashi, *Nature*, 1993, **363**, 603–605.

3 J. A. Robinson, E. S. Snow, S. C. Badescu, T. L. Reinecke and F. K. Perkins, *Nano Lett.*, 2006, **6**, 1747–1751.

4 Y. Miyauchi, M. Iwamura, S. Mouri, T. Kawazoe, M. Ohtsu and K. Matsuda, *Nat. Photonics*, 2013, **7**, 715–719.

5 K. Gong, F. Du, Z. Xia, M. Durstock and L. Dai, *Science*, 2009, **323**, 760–764.

6 S. Yasuda, L. Yu, J. Kim and K. Murakoshi, *Chem. Commun.*, 2013, **49**, 9627–9629.

7 S. Yasuda, A. Furuya, Y. Uchibori, J. Kim and K. Murakoshi, *Adv. Funct. Mater.*, 2016, **26**, 738-744.

8 X. Cui, M. Freitag, R. Martel, L. Brus and P. Avouris, *Nano Lett.*, 2003, **3**, 783–787.

9 Y. Miyato, K. Kobayashi, K. Matsushige and H. Yamada, *Nanotechnology*, 2007, **18**, 084008.

10 S. Yasuda, K. Ikeda, L. Yu and K. Murakoshi, *Jpn. J. Appl. Phys.*, 2012, **51**, 08KB06.

11 M. J. O' Connell, E. E. Eibergen and S. K. Doorn, *Nat. Mater.*, 2005, **4**, 412–418.

12 Y. Tanaka, Y. Hirana, Y. Niidome, K. Kato, S. Saito and N. Nakashima, *Angew. Chemie - Int. Ed.*, 2009, **48**, 7655–7659.

13 M. Kalbac, H. Farhat, L. Kavan, J. Kong, K. Sasaki, R. Saito and M. S. Dresselhaus, *ACS Nano*, 2009, **3**, 2320–2328.

14 K. Okazaki, Y. Nakato and K. Murakoshi, *Phys. Rev. B*, 2003, **68**, 035434.

15 M. Fleischmann, P. J. Hendra and a J. McQuillan, *Chem. Phys. Lett.*, 1974, **26**, 163–166.

16 Y. Sawai, B. Takimoto, H. Nabika, K. Ajito and K. Murakoshi, *J. Am. Chem. Soc.*, 2007, **129**, 1658–1662.

17 E. C. Le Ru and P. G. Etchegoin, *Principles of Surface-Enhanced Raman Spectroscopy*, Elsevier, 2009.

18 F. Nagasawa, M. Takase, H. Nabika and K. Murakoshi, *Chem. Commun.*, 2011, **47**, 4514–4516.

19 T. Konishi, M. Kiguchi, M. Takase, F. Nagasawa, H. Nabika, K. Ikeda, K. Uosaki, K. Ueno, H. Misawa and K. Murakoshi, *J. Am. Chem. Soc.*, 2013, **135**, 1009–1014.

20 K. Kneipp, A. Jorio, H. Kneipp, S. D. M. Brown, K. Shafer, J. Motz, R. Saito, G. Dresselhaus and M. S. Dresselhaus, *Phys. Rev. B*, 2001, **63**, 081401.

21 N. Hayazawa, T. Yano, H. Watanabe, Y. Inouye and S. Kawata, *Chem. Phys. Lett.*, 2003, **376**, 174–180.

22 M. Takase, H. Nabika, S. Hoshina, M. Nara, K.-I. Komeda, R. Shito, S. Yasuda and K. Murakoshi, *Phys. Chem. Chem. Phys.*, 2013, **15**, 4270–4274.

23 M. Takase, H. Ajiki, Y. Mizumoto, K. Komeda, M. Nara, H. Nabika, S. Yasuda, H. Ishihara and K. Murakoshi, *Nat. Photonics*, 2013, **7**, 550–554.

24 J. C. Hulteen, *J. Vac. Sci. Technol. A Vacuum, Surfaces, Film.*, 1995, **13**, 1553.

25 S. Maruyama, R. Kojima, Y. Miyauchi, S. Chiashi and M. Kohno, *Chem. Phys. Lett.*, 2002, **360**, 229–234.

26 H. Kataura, Y. Kumazawa, Y. Maniwa, I. Umezu, S. Suzuki, Y. Ohtsuka and Y. Achiba, *Synth. Met.*, 1999, **103**, 2555–2558.

27 P. T. Araujo, S. K. Doorn, S. Kilina, S. Tretiak, E. Einarsson, S. Maruyama, H. Chacham, M. a. Pimenta and A. Jorio, *Phys. Rev. Lett.*, 2007, **98**, 1–4.

28 L. Kavan, P. Rapta, L. Dunsch, M. J. Bronikowski, P. Willis and R. E. Smalley, *J. Phys. Chem. B*, 2001, **105**, 10764–10771.

29 P. W. Ruch, L. J. Hardwick, M. Hahn, A. Foelske, R. Kötz and A. Wokaun, *Carbon*, 2009, **47**, 38–52.

30 Y. Akai and S. Saito, *Phys. E Low-dimensional Syst. Nanostructures*, 2005, **29**, 555–559.

31 S. Trasatti and O. A. Petrii, *Pure Appl. Chem.*, 1991, **63**, 711–734.

32. Y. Marcus, *Ion Solvation*, p256, John Wiley & Sons Ltd., 1985.

33 J. M. Simmons, B. M. Nichols, S. E. Baker, M. S. Marcus, O. M. Castellini, C.-S. Lee, R. J. Hamers and M. A. Eriksson, *J. Phys. Chem. B*, 2006, **110**, 7113–7118.

34 R. Ma, D. Yoon, K.-Y. Chun and S. Baik, *Chem. Phys. Lett.*, 2009, **474**, 158–161.

35 P. P. Pal, T. Larionova, I. V. Anoshkin, H. Jiang, M. Nisula, A. A. Goryunkov, O. V. Tolochko, M. Karppinen, E. I. Kauppinen and A. G. Nasibulin, *J. Phys. Chem. C*, 2015, **119**, 27821–27828.

36 H. Xia, Y. Zhang, C. Chen, W. Wu, K. Yao and J. Zhang, *J. Mater. Sci. Technol.*, 2016, **32**, 533-538.